


# Histologic Examination of Vocal Fold Mucosal Wave and Vibration

Hye Rhyn Chung, BS ; Neha K. Reddy, BA ; Daniel Manzoor, MD; Patrick Schlegel, PhD;  
 Zhaoyan Zhang, PhD ; Dinesh K. Chhetri, MD

**Objectives:** Despite gross anatomic and histologic differences between human and canine vocal folds, similar wave patterns have been described yet not fully characterized. We reconstructed vocal fold (VF) vibration in a canine hemilarynx and performed histologic examination of the same vocal fold. We demonstrate comparable wave patterns while exploring the importance of certain anatomic architectures.

**Methods:** An *in vivo* canine hemilarynx was phonated against a glass prism at low and high muscle activation conditions. Vibration was captured using high-speed video, and trajectories of VF medial surface tattooed landmarks were 3D-reconstructed. The method of empirical eigenfunctions was used to capture the essential dynamics of vibratory movement. Histologic examination of the hemilarynx was performed.

**Results:** Oscillation patterns were highly similar between the *in vivo* canine and previous reports of *ex vivo* human models. The two most dominant eigenfunctions comprised over 90% of total variance of movement, representing opening/closing and convergent/divergent movement patterns, respectively. We demonstrate a vertical phase difference during the glottal cycle. The time delay between the inferior and superior VF was greater during opening than closing for both activation conditions. Histological examination of canine VF showed not only a thicker lamina propria layer superiorly but also a distinct pattern of thyroarytenoid muscle fibers and fascicles as described in human studies.

**Conclusions:** Histologic and vibratory examination of the canine vocal fold demonstrated human vocal fold vibratory patterns despite certain microstructural differences. This study suggests that the multilayered lamina propria may not be fundamental to vibratory patterns necessary for human-like voice production.

**Key Words:** empirical eigenfunction, mucosal wave, thyroarytenoid muscle, voice production, vocal fold histology.

**Level of Evidence:** NA (Basic science study)

*Laryngoscope*, 134:264–271, 2024

## INTRODUCTION

The larynx is a biological organ with a mechanical role to function as an energy converter, converting aerodynamic energy into sound energy. Sound is produced when a threshold subglottal pressure against the adducted vocal folds (VFs) is reached and they begin to vibrate.<sup>1</sup> Superior and recurrent laryngeal nerves (SLN and RLN) innervate both VFs, which regulate elongation and adduction of the VFs respectively. The VFs themselves consist of distinct layers, divided biomechanically between the cover (epithelium and superficial plus intermediate lamina propria layers) and body layers (deep lamina propria layer and the thyroarytenoid muscle), which interact during vibration to generate the traveling mucosal wave on the VF surface.<sup>2</sup> The propagation of the mucosal wave is fundamental to

vocalization and is believed to rely on the biomechanical properties of the various structures of the VFs.<sup>3,4</sup> Characterization of these properties and their roles in mucosal wave propagation and VF oscillation is therefore germane to understanding laryngeal function and treating laryngeal diseases.

Hirano's characterization of human VF histology and the subsequent cover-body theory of phonation has provided the framework for research in laryngeal biomechanics.<sup>2</sup> Namely, differential stiffness conditions in the body versus cover layer are considered to have an important role in vibratory dynamics and voice production. Although VF stiffness is primarily regulated by activation of the cricothyroid (CT) and thyroarytenoid (TA) muscles, micromolecular composition also serves a foundational role.<sup>5</sup> For example, it has been proposed that fibrous proteins such as collagen and elastin contribute to the tensile stress-strain characteristics of the VFs,<sup>6</sup> whereas proteoglycans and hyaluronic acid (HA) contribute to the viscoelastic shear properties of the extracellular matrix (ECM).<sup>7,8</sup> Furthermore, muscle fiber structure, orientation, density, and alignment are also of importance.<sup>9,10</sup> Alterations to the VF's structural components therefore affect its biomechanical properties, potentially resulting in aberrant oscillation and dysphonic voice.

The use of the canine model enabled *in vivo* exploration of VF vibration. However, gross anatomic and histologic differences from human VFs have been described. Kurita proposed that the canine VF cover layer has a

From the David Geffen School of Medicine (H.R.C., N.K.R.), University of California, Los Angeles, California, USA; Department of Pathology (D.M.), University of California, Los Angeles, California, USA; and the Department of Head and Neck Surgery (P.S., Z.Z., D.K.C.), University of California, Los Angeles, California, USA.

Editor's Note: This Manuscript was accepted for publication on July 18, 2023.

The authors have no other funding, financial relationships, or conflicts of interest to disclose.

This manuscript was presented as a podium presentation at the Triological Society Combined Sections Meeting in Coronado, CA on Jan 27th, 2023

Send correspondence to Dinesh K. Chhetri, 62-132 CHS, 10833 Le Conte Avenue, Los Angeles, CA 90095, USA. Email: [dchhetri@mednet.ucla.edu](mailto:dchhetri@mednet.ucla.edu)

DOI: 10.1002/lary.30928

two-layer structure with no vocal ligament,<sup>4</sup> whereas Garrett et al. described a three-layer structure similar to humans.<sup>11</sup> Hahn et al. found that the canine VF contains a band of elastin fibers deep to the subepithelial basement membrane zone, a much thicker VF cover layer and up to four times more HA in the lamina propria layer compared with human VF.<sup>12</sup> Conversely, the human VF cover layer is composed of a three-layer structure with a higher elastin content in the deeper layers of the lamina propria. These differences impact their respective viscoelastic properties, with the canine VF cover being significantly more viscous than the human VF cover.<sup>13</sup>

Although these previous studies outlined general structure–function interactions, which specific structure–function relationships are necessary to achieve human-like phonation remains largely unexplored. Furthermore, recent computational analyses have failed to show a direct cause–effect relationship between varying VF stiffness and the four voice types laid out by Hirano,<sup>2,14</sup> calling into question the significance of the layered VF structure for glottal dynamics as well as the utilization of higher-order models of phonation in the study of voice production.<sup>14</sup> Ultimately, elucidation of the significance of specific components of VF structure to its oscillation patterns requires comparative studies that analyze VF histology and vibration; however, few exist in the literature. Garret et al. previously conducted a comparative study of human, canine, monkey, and pig larynges and found the histology, mucosal wave propagation, and vertical phase difference in canine VF vibration were most similar to that of humans.<sup>11</sup> However, endoscopic videostroboscopy was employed allowing for visualization of VF vibrations from a superior view, which precluded the ability to examine the crucial medial surface dynamics of the VFs. More recently, three-dimensional (3D) reconstruction of the VF medial surface vibration using an *in vivo* hemilarynx has made it possible to directly characterize critical components of mucosal wave propagation and the vertical phase delay with high accuracy.<sup>15</sup> This methodology additionally

allows studying of VF phonation as a function of laryngeal nerve activation for further vibratory characterization.

In this study, we analyze VF vibratory dynamics in the context of VF microanatomy by capturing VF medial surface vibration in an *in vivo* canine hemilarynx phonation model, reconstructing the 3D deformation of VF tissue during vibration and transposing vibratory behavior with histologic examination of the same larynx. We demonstrate comparable vibratory patterns in canine phonation to human phonation, while discussing the potential importance of microanatomical structure.

## MATERIALS AND METHODS

### *In Vivo Canine Hemilarynx Phonation*

This study was approved by the Institutional Animal Research Committee and in compliance with all applicable national and institutional policies on the use of laboratory animals. Hemilarynx surgery and *in vivo* hemilaryngeal phonation has been detailed previously.<sup>16</sup> In brief, a mongrel *in vivo* canine larynx was exposed via an infrahyoid pharyngotomy, and a right hemilaryngectomy was performed. Cuff electrodes (Ardiem Medical, Indiana, PA) were connected to exposed SLN and RLN for electrical stimulation. A transparent right-angle glass prism was positioned with the base along the glottal midline. The two sides of the right-angle prism provided two distinct views of the VF medial surface (Fig. 1A) that were captured with a high-speed video camera (Phantom v210, Vision Research Inc., Wayne, NJ) at 3,000 fps. A subglottal tube provided rostral airflow to induce phonation. VF oscillations against the glass prism were recorded for 3D reconstruction.

During phonation, SLN and RLN were stimulated over 10 graded levels to activate VF elongation and adduction from threshold (hint of muscle reaction: level 1) to maximum activation (no change in muscle reaction with further increase in stimulation: level 10). For illustrative purposes, two stimulation conditions were chosen for analysis: (1) Threshold activation of RLN only (SLN0/RLN1) to capture VF oscillation state with minimal tissue stiffness and (2) maximum activation of SLN and RLN (SLN10/RLN10) to represent VF oscillation at maximum tissue stiffness.

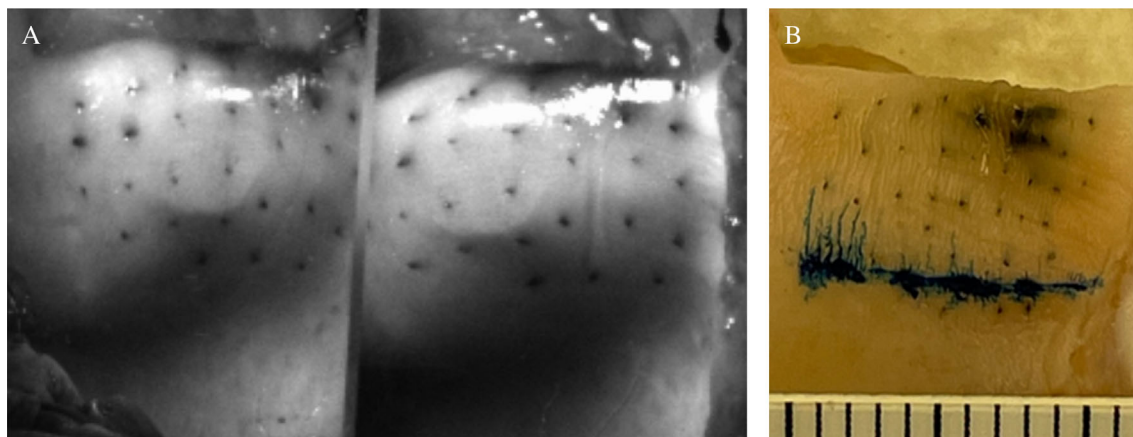


Fig. 1. (A) Still frame from high-speed video of the medial vocal fold phonating against a right-angle glass prism. The two faces of the prism provided two distinct views of the grid of tattooed landmarks on the medial VF surface that was tracked for 3D reconstruction of glottal deformation and used to visualize the location of mucosal wave upheaval origin. (B) Hemilarynx used for phonation prepared for histologic examination. Anterior–posterior mucosal cut was made at the location of the origin of mucosal upheaval with a scalpel and inked with blue dye as a reference point (ruler markings are in millimeters).

### 3D Reconstruction of VF Medial Surface Trajectories

To track the 3D movements of the VF medial surface, a grid of 30 India ink landmarks (7 columns, 3–5 rows per column, Fig. 1B) was tattooed onto the left VF medial surface. Landmarks were tracked using a custom software tool (GLabel, Friedrich Alexander University Erlangen-Nürnberg), and 3D reconstruction of landmark positions was performed using an algorithm developed and validated in-house for this setup.<sup>16</sup> The mid-membranous column of landmarks was tracked over three continuous glottal cycles, and the cyclical trajectories of each axial level of the medial VF were depicted in the coronal plane.

Empirical eigenfunctions (EEFs) were used to capture and display the essential dynamics of VF movement and de-noise trajectories. EEFs are a commonly used tool to separate complex 3D vibratory dynamics into essential one-dimensional patterns of movement. Spatial and temporal EEFs describe one-dimensional movement directions and amplitudes. The first pair of spatial and temporal EEFs (EEF1) represents the one-dimensional movement that captures the greatest share of variance of the full 3D movement. Analogously, the second pair (EEF2) captures the movement pattern with the second greatest share of total variance. A more detailed explanation is provided in Döllinger et al.<sup>17</sup> All evaluations were performed using Matlab (version 9.11.0.1809720 (R2021b) Update 1).

### Tissue Preparation

Immediately following *in vivo* phonation experiments, the larynx was removed and placed in formalin until histologic

analysis. Prior to histologic processing, a scalpel was used to make a small mucosal incision in the anteroposterior direction at the determined location of the origin of the mucosal wave and marked with blue ink for reference (Fig. 1B). The location of the origin of the mucosal wave upheaval was determined based on review of HSV recordings. A 3 mm coronal section from the mid-membranous VF was cut and then processed and embedded in paraffin. Then, 4  $\mu$ m sections were cut via a microtome and mounted on glass slides, which were examined microscopically using Elastic Masson Trichrome (EMT) stain.

## RESULTS

### Vibratory Trajectory and EEFs

Figure 2A–C depicts EEFs for activation condition SLN0/RLN1 along with reconstructed trajectories using only (A) EEF1, (B) EEF1, and 2 and (C) EEF 1 through 3. Analogously, Figure 2D–F depicts the same for activation condition SLN10/RLN10. EEFs are visualized with arrows that indicate direction and amplitude of EEF-based trajectory motion. Solid and dotted lines connecting arrow tips and bases are indicators of EEF-dependent surface shape at cycle extrema.

EEF1 accounted for 66% of variance in activation condition SLN0/RLN1 and 56% of variance in activation condition SLN10/RLN10 and captured synchronal opening and closing of the vocal fold. EEF2 captured 30% and 34% of variance, respectively, and depicts the convergent/divergent shape

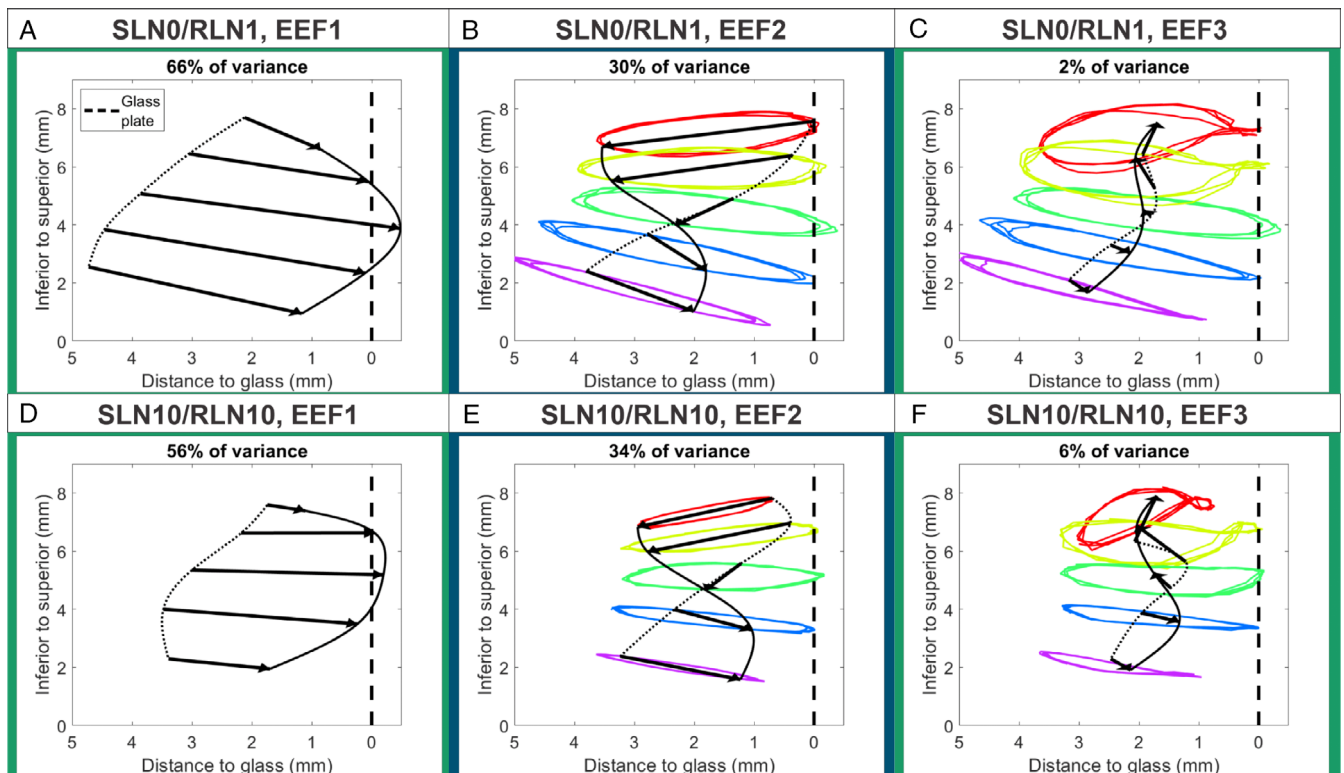


Fig. 2. EEFs for low activation condition SLN0/RLN1 with reconstructed trajectories using (A) EEF1, (B) EEF1-2, and (C) EEF1-3. Figures D-F depict analogous reconstructions for high activation condition SLN10/RLN10. For both activation conditions, EEF1 captured synchronal opening and closing movements of the vocal fold and EEF2 captured an out-of-phase, convergent/divergent movement between the inferior and superior vocal fold, demonstrating the vertical phase difference during vibration. Finally, EEF3 contributed to the figure-8 shape pattern of superior vibration in condition SLN10/RLN10.

during opening and closing of the VF. EEF3 captured 2% and 6% of variance, respectively, and contributed to the figure-8 shape pattern of superior vibration in condition SLN10/RLN10.

### Vibratory Trajectory in Relation to VF Histology

Figure 3 illustrates trajectories of each landmark over three oscillation cycles for activation conditions SLN0/RLN1 (Fig. 3A,B) and SLN10/RLN10 (Fig. 3C,D) with and without histologic section overlay. In both activation conditions, the most superior landmark (red) displayed a predominantly circular trajectory. Histologically, this axial level corresponded to the area of the VF where the TA muscle was furthest from the epithelial surface (Fig. 3B,D). Interstitial fluid and a network of matrix at this level represent the lamina propria layer which is also thickest at this level. In contrast, the most inferior landmark (purple) exhibited a highly eccentric elliptical, mediolateral trajectory. This level was nearest to our marked origin of mucosal upheaval, which was also the site where the TA muscle was

closest to the epithelium, a finding previously demonstrated by Yumoto et al.<sup>18</sup>

### Lateral and Vertical Displacements

Maximum lateral and vertical displacements of each trajectory for both activation conditions are given in Table I. Lateral displacement increased from superior to inferior in condition SLN0/RLN1 reaching a maximum of 5 mm. In contrast, maximum lateral displacement for SLN10/RLN10 was 3.5 mm with no clear increasing trend. Vertical displacements in SLN0/RLN1 were very similar across axial landmarks, whereas vertical displacements in SLN10/RLN10 decreased from superior to inferior.

### Time Delay Between Inferior and Superior VF during Glottal Cycle

Figure 4 shows mediolateral excursions (distance from midline glass plate) of an inferior (blue) and a superior (yellow) VF surface landmark plotted over time for both activation conditions. The glottal cycle length for low

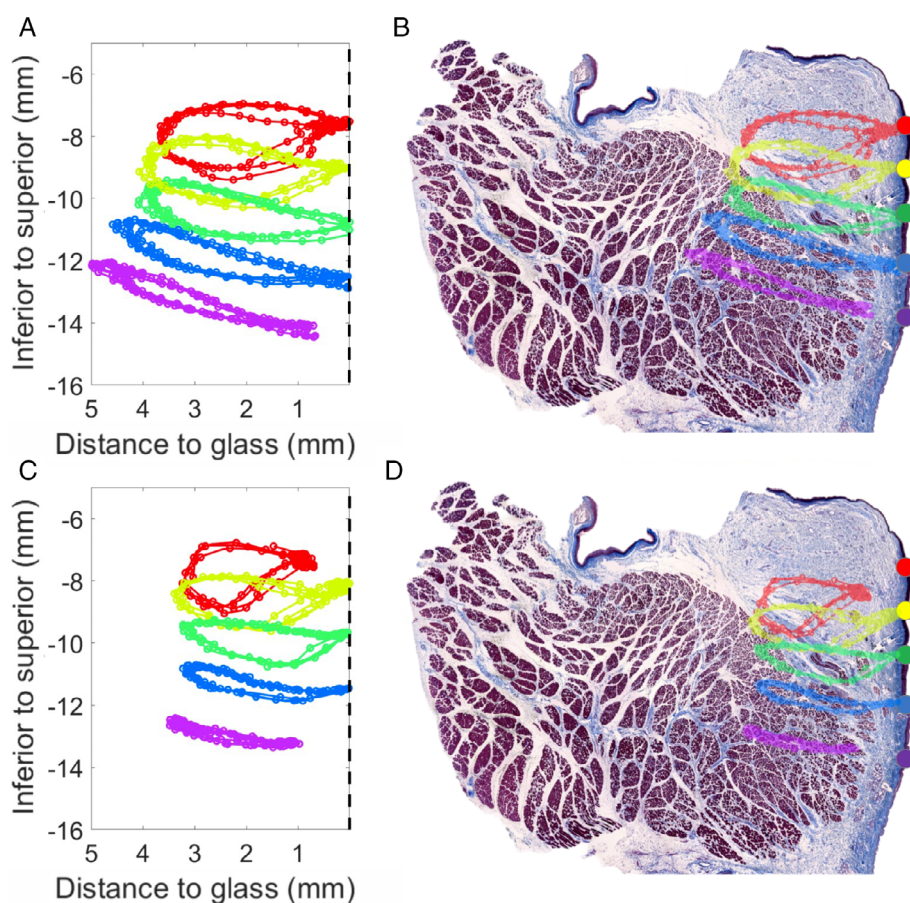


Fig. 3. (A) Trajectories of each superior–inferior medial surface landmark over three full oscillation cycles for activation conditions SLN0/RLN1 (A,B) and SLN10/RLN10 (C,D), without (A,C) and with (B,D) histologic section overlay. Dashed vertical black line at 0 mm represents the glass prism at the glottal midline. For both conditions, the most superior landmark (red) displayed a predominantly circular trajectory, and at this level, the lamina propria was thickest. The most inferior landmark (purple) exhibited a highly eccentric elliptical, mediolateral trajectory. At this medial surface level, the thyroarytenoid muscle came closest to the epithelium.

TABLE I.  
Maximum Lateral and Vertical Displacements of All Five Trajectories for the Illustrative Low and High Muscle Activation Conditions.

Maximum trajectory displacements (mm) by activation condition				
Landmark location	SLN0/RLN1 (lateral)	SLN10/RLN10 (lateral)	SLN0/RLN1 (vertical)	SLN10/RLN10 (vertical)
1 (most superior)	3.7	3.2	2.5	2.3
2	4.1	3.4	2.3	1.8
3	4.1	3.2	2	1.5
4	4.6	3.2	2.2	1.2
5 (most inferior)	5	3.5	2.4	0.9

Landmark locations are along the coronal mid-membranous plane.

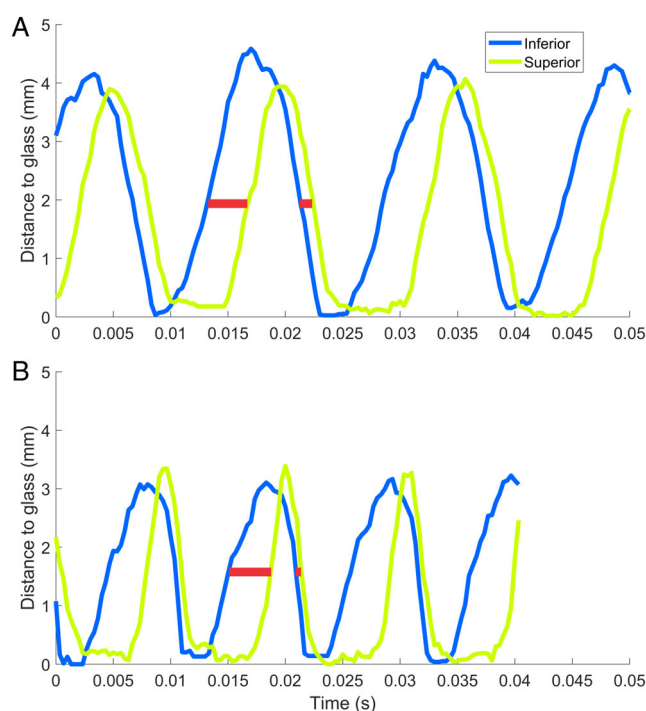


Fig. 4. Vertical phase difference between the inferior and superior glottis over three glottal cycles is represented by an out-of-phase mediolateral displacement of inferior (blue) and superior (yellow) surface landmarks over time (s) for activation conditions (A) SLN0/RLN1 and (B) SLN10/RLN10. Time delay in closing and opening between the inferior and superior glottis was longer during the opening phase in comparison to the closing phase (red bars) for both activation conditions. Mediolateral displacement was measured as the distance between the medial surface landmark and the glass prism in mm as in Figure 3.

and high activation conditions was approximately 14 and 10 ms, respectively. The vertical distance between these two landmarks was on average 2.9 mm. The time delay between the two landmarks during opening was 3.33 ms for both low and high activation conditions. However, the time delay between the two landmarks, represented by

the length of red bars in Figure 4, during closing was 1.33 and 0.67 ms for the low and high activation conditions, respectively. This yields a rough estimation of vertical opening speeds of 0.87 m/s for both conditions and closing speeds of 2.18 and 4.33 m/s for the low and high activation conditions, respectively.

## Histology

The histologic section of the VF is shown in Figure 5A. The TA muscle measured approximately 10 mm × 7 mm in the transverse and vertical directions, respectively. The TA muscle came to its most superficial point, closest to the epithelium, at the observed origin of the mucosal wave (black box in Fig. 5A). The distance between the muscle and the epithelial surface was approximately 0.5 mm at this location and gradually increased in the superior direction such that the lamina propria layer was thickest at the superior margin of the VF. Consistent with previous reports, this LP layer measured much thicker than that observed in human VFs.<sup>11</sup> The mucosal incision at the location of mucosal wave origin is shown in Figure 5B. Subepithelial mucous glands (black arrow) were present throughout the subglottis below this level but were abruptly absent above.

Distinct patterns of TA muscle fibers and fascicles could be appreciated. The TA muscle was divided into superior medial (SM), inferior medial (IM), superior lateral (SL), and inferior lateral (IL) quadrants (Fig. 5A and 6) based on these observations. The SM quadrant contained a large array of small diameter muscle fascicles with heterogeneously sized, small-diameter muscle fibers arranged in a loose organization within each fascicle (Fig. 6). The IM quadrant also contained heterogeneously sized fibers but demonstrated larger muscle fascicles compared to the SM quadrant. The lateral quadrants demonstrated the largest fascicles with densely packed and homogeneously sized muscle fibers but with more interfascicular connective tissue.

## DISCUSSION

In this study, we investigated vibratory dynamics and histological microanatomy in a canine *in vivo* model. Although there are anatomic and structural differences between canine and human larynges, we demonstrate vibratory dynamics in the canine model that are very similar to oscillation patterns observed in human *ex vivo* models. This calls into question the importance of the unique three-layered structure of the human larynx in terms of fundamental oscillatory behavior.

A common argument against utilizing the canine larynx as a model for human phonation is the absence of a three-layer VF structure and vocal ligament and the presence of a significantly thicker LP layer. It has been argued that these structural differences preclude the ability for canine larynges to display vibratory patterns necessary for human phonation. For instance, Alipour-Haghighi and Titze theorized that the absence of a vocal ligament would render the cover layer too stiff to propagate the mucosal wave at high fundamental frequencies.<sup>19</sup> Kimura et al. further

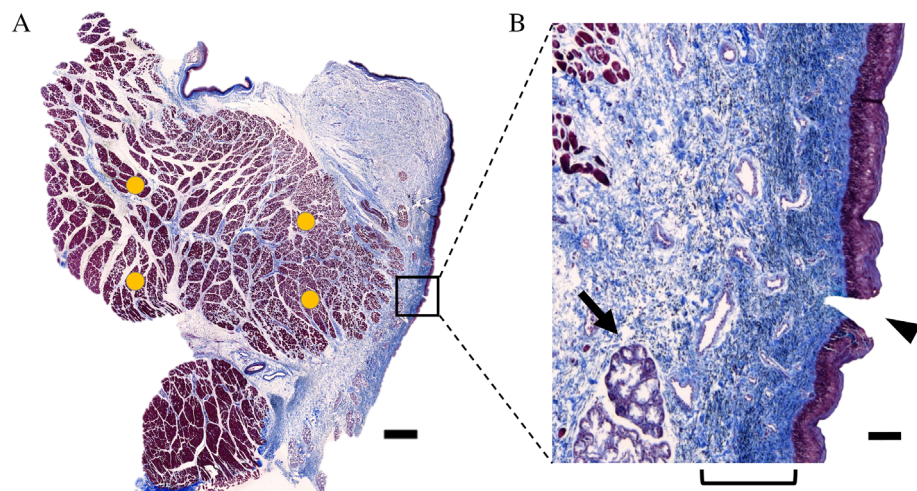


Fig. 5. (A) Histologic section of the entire vocal fold. The location of the origin of mucosal upheaval is represented by the small black box. Four circles indicate the locations of the thyroarytenoid muscle shown in high-power view in Figure 5, representing the superior medial, inferior medial, superior lateral, and inferior lateral subdivisions of the thyroarytenoid muscle (scale bar 1 mm). (B) High-power view of the location of the black box in panel A. The location of the mucosal upheaval is represented by the black arrowhead.

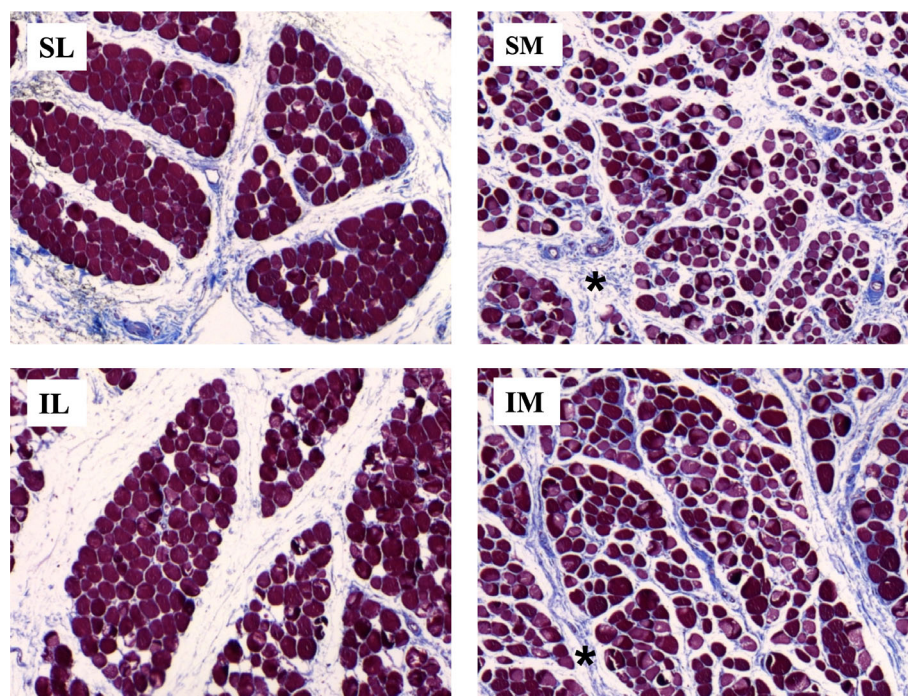


Fig. 6. The thyroarytenoid muscle was divided into superior medial (SM), inferior medial (IM), superior lateral (SL), and inferior lateral (IL) quadrants (see Figure 5A). The SM quadrant contained heterogeneous, small diameter muscle fibers, and small muscle fascicles. Muscle fibers were arranged loosely within each fascicle in this quadrant. The IM quadrant also contained heterogeneously sized muscle fibers but with larger fascicles compared with the SM quadrant. The SL and IL quadrants contained large diameter muscle fascicles, and homogeneous large diameter muscle fibers that were densely arranged within each fascicle.

suggested that higher viscosity of the canine cover would require greater phonation threshold pressures to set the VFs into vibration, particularly for large-amplitude vibrations.<sup>13</sup> However, Chhetri et al. demonstrated a nearly 4 octave pitch range for canine phonation as well as comparable threshold subglottal pressures of 0.2–0.3 kPa using a

full larynx *in vivo* phonation methodology.<sup>20</sup> Therefore, both input and output signals are comparable to human phonation. Taken together, previous studies and findings in our current study showed that although there are distinct differences between canine and human larynges, some other features shared by both canine and humans may have a

larger impact on oscillation patterns. In particular, the canine TA has been shown to be most histologically similar to human TA muscle. Sanders et al.'s characterization of the human superior medial TA muscle fibers is demonstrated by the canine TA in our current study, suggesting that the TA may be highly responsible for observed mucosal wave characteristic seen in humans and canines.<sup>9</sup> Further support for this notion is provided by computational analyses that showed a small effect of both (1) longitudinal stiffness differential between the body and cover layers and (2) the medial–lateral depth of the cover layer.<sup>14,21</sup> Instead, these studies demonstrated the importance of VF vertical thickness and transverse stiffness in the coronal plane, both features mediated by the TA muscle. These features ultimately modulate glottal shape, closure patterns, and resistance against subglottal pressures, which are all necessary for voice production.<sup>14</sup>

In our *in vivo* hemilarynx experiment, the first two EEFs captured more than 90% of total variance, consistent with Döllinger et al.'s *ex vivo* human experiments.<sup>17</sup> Additional similarities include the trajectories being more circular superiorly and more ellipsoid or line-like inferiorly and observation of “figure-eight” shaped oscillation patterns in EEFs superiorly. In contrast to the *ex vivo* human study, the roles of EEF1 and EEF2 were reversed in our study, where EEF1 captured synchronal opening and closing and EEF2 captured the convergent/divergent shape during the glottal cycle. This discrepancy may be due to our use of an *in vivo* model and considerably higher airflow used in our experiments (1500 ml/s vs. 400 ml/s maximum in the *ex vivo* human study) that resulted in larger oscillation amplitudes and lateral/vertical displacements of the vocal fold (Table I). However, overall observed oscillation patterns are highly similar between the *in vivo* canine and *ex vivo* human models.

The vertical phase difference seen in VF vibration (Fig. 4) is a fundamental aspect of normal phonation and is considered a key component of mucosal wave propagation.<sup>21,22</sup> In our experiment, the observed speed of the vertically travelling wave was similar to reported human mucosal wave speeds during opening (in a range between 0.5 and 2 m/s)<sup>23,24</sup> and faster during closing, especially for high nerve activation conditions. The vertical delay was more pronounced during opening than during closing in both stimulation conditions. Although this pattern of a larger time delay between superior and inferior vocal fold during opening than during closing has been demonstrated in computational models,<sup>25</sup> this specific aspect of vibratory movement has not been experimentally validated. Furthermore, previous characterizations of the vertical phase difference were taken over the entire length of the glottal cycle without distinguishing between opening and closing phases.<sup>25</sup>

Study limitations include the use of only a single larynx due to the complexity of the experiment and a recording frame rate of 3000 fps that restricted temporal resolution of especially the closing phase. In addition, with our medial surface visualization technique, the vibratory patterns could only be tracked on the VF surface and not deep within the tissue. Finally, only a small number of nerve activation conditions were

analyzed. Further experiments are needed to address these study limitations.

## CONCLUSION

This study investigated the histologic correlates of VF vibration, exploring the importance of anatomic architecture in the biomechanics of sound production. We demonstrated similar oscillatory behavior in the *in vivo* canine model to human *ex vivo* models, despite distinct microstructural differences. Future studies on more larynges featuring higher recording frame rates are needed to track closing behavior of the canine model.

## FUNDING INFORMATION

This study was supported by Grant No. RO1 DC011300 from the National Institutes of Health.

## BIBLIOGRAPHY

- Azar SS, Chhetri DK. Phonation threshold pressure revisited: effects of intrinsic laryngeal muscle activation. *Laryngoscope*. 2022;132(7):1427-1432. <https://doi.org/10.1002/lary.29944>.
- Hirano M. Morphological structure of the vocal cord as a vibrator and its variations. *Folia Phoniatr*. 1974;26:89-94.
- Krausert CR, Olszewski AE, Taylor LN, McMurray JS, Dailey SH, Jiang JJ. Mucosal wave measurement and visualization techniques. *J Voice*. 2011; 25(4):395-405. <https://doi.org/10.1016/j.jvoice.2010.02.001>.
- Kurita S, Nagata K, Hirano M. A comparative study of the layer structure of the vocal fold. In: Bless D, Abbs J, eds. *Vocal Fold Physiology: Contemporary Research and Clinical Issues*. San Diego, CA: College Hill Press; 1983:3-21.
- Hirano M, Kakita Y, Ohmaru K, Kurita S. Structure and mechanical properties of vocal fold. *Speech Lang*. 1982;7:271-297.
- Hammond TH, Zhou R, Hammond EH, Pawlak A, Gray SD. The intermediate layer: a morphologic study of the elastin and hyaluronic acid constituents of normal human vocal folds. *J Voice*. 1997;11(1):59-66. [https://doi.org/10.1016/s0892-1997\(97\)80024-0](https://doi.org/10.1016/s0892-1997(97)80024-0).
- Gray SD, Titze IR, Chan R, Hammond TH. Vocal fold proteoglycans and their influence on biomechanics. *Laryngoscope*. 1999;109(6):845-854. <https://doi.org/10.1097/00005537-199906000-00001>.
- Zhang Z. Structural constitutive modeling of the anisotropic mechanical properties of human vocal fold lamina propria. *J Acoust Soc Am*. 2019; 145(6):EL476-EL482. <https://doi.org/10.1121/1.5109794>.
- Sanders I, Rai S, Han Y, Biller HF. Human vocalis contains distinct superior and inferior subcompartments: possible candidates for the two masses of VF vibration. *Ann Otol Rhinol Laryngol*. 1998;107(10 Pt 1):826-833. <https://doi.org/10.1177/000348949810701003>.
- Rosenfield DB, Miller RH, Sessions RB, Patten BM. Morphologic and histochemical characteristics of laryngeal muscle. *Arch Otolaryngol*. 1982; 108(10):662-666. <https://doi.org/10.1001/archotol.1982.00790580056018>.
- Garrett CG, Coleman JR, Reinisch L. Comparative histology and vibration of the vocal folds: implications for experimental studies in microlaryngeal surgery. *Laryngoscope*. 2000;110(5 Pt 1):814-824. <https://doi.org/10.1097/00005537-200005000-00011>.
- Hahn MS, Kobler JB, Starcher BC, Zeitels SM, Langer R. Quantitative and comparative studies of the vocal fold extracellular matrix. I: elastic fibers and hyaluronic acid. *Ann Otol Rhinol Laryngol*. 2006;115(2):156-164. <https://doi.org/10.1177/000348940611500213>.
- Kimura M, Mau T, Chan RW. Rheometric properties of canine vocal fold tissues: variation with anatomic location. *Auris Nasus Larynx*. 2011;38(3): 367-372. <https://doi.org/10.1016/j.anl.2010.09.006>.
- Zhang Z. Effect of vocal fold stiffness on voice production in a three-dimensional body-cover phonation model. *J Acoust Soc Am*. 2017;142(4): 2311-2321. <https://doi.org/10.1121/1.5008497>.
- Doellinger M, Berry DA, Berke GS. A quantitative study of the medial surface dynamics of an *in vivo* canine vocal fold during phonation. *Laryngoscope*. 2005;115(9):1646-1654. <https://doi.org/10.1097/01.mlg.00001175068.25914.61>.
- Reddy NK, Schlegel P, Lee Y, Chhetri DK. 3D reconstruction of Phonatory glottal shape and volume: effects of neuromuscular activation. *Laryngoscope*. 2023;133(2):357-365. <https://doi.org/10.1002/lary.30178>.
- Döllinger M, Tayama N, Berry DA. Empirical Eigenfunctions and medial surface dynamics of a human vocal fold. *Methods Inf Med*. 2005;44(3): 384-391.
- Yumoto E, Kadota Y, Kurokawa H. Tracheal view of vocal fold vibration in excised canine larynges. *Arch Otolaryngol Head Neck Surg*. 1993;119(1): 73-78. <https://doi.org/10.1001/archotol.1993.01880130075011>.

19. Alipour-Haghighi F, Titze IR. Elastic models of vocal fold tissues. *J Acoust Soc Am.* 1991;90(3):1326-1331. <https://doi.org/10.1121/1.401924>.
20. Chhetri DK, Neubauer J, Berry DA. Neuromuscular control of fundamental frequency and glottal posture at phonation onset. *J Acoust Soc Am.* 2012; 131(2):1401-1412. <https://doi.org/10.1121/1.3672686>.
21. Zhang Z. Contribution of laryngeal size to differences between male and female voice production. *J Acoust Soc Am.* 2021;150(6):4511-4521. <https://doi.org/10.1121/10.0009033>.
22. Zhang Z. Mechanics of human voice production and control. *J Acoust Soc Am.* 2016;140(4):2614-2635. <https://doi.org/10.1121/1.4964509>.
23. Stevens KN. *Acoustic Phonetics.* Cambridge (MA): The MIT Press; 1998.
24. Titze IR, Jiang JJ, Hsiao TY. Measurement of mucosal wave propagation and vertical phase difference in vocal fold vibration. *Ann Otol Rhinol Laryngol.* 1993;102(1 Pt 1):58-63. <https://doi.org/10.1177/000348949310200111>.
25. Boessenecker A, Berry D, Lohscheller J, et al. Mucosal wave properties of a human vocal fold. *Acta Acust United Acust.* 2007;93:815-823.